Molecular Crystals and Liquid Crystals
Publication details, including instructions for authors and subscription information:
http://www.tandfonline.com/loi/gmcl16

Structure and Paramagnetism of Strong Charge-Transfer Complexes: 5.10-Dihydro-2.3.5.7.8.10-hexamethylphenazine-tetracyanoethylene (M_6P) (TCNE)

S. Flandrois [a] , K. Ludolf [b] , H. J. Keller [b] , D. Nöthe [b] , S. R. Bondeson [c] , Z. G. Soos [d] & D. Wehe [b]

[a] CNRS-CRPP, Domaine Universitaire, Talence, France

[b] Anorganisch-Chemisches Institut der Universität. Heidelberg, D-6900, Heidelberg, 1, GFR

[c] Department of Chemistry, University of Wisconsin, Stevens Point, Wl, 54481, USA

[d] Department of Chemistry, Princeton University, Princeton, N.J., 08544, USA

Version of record first published: 20 Apr 2011.

Mol. Cryst. Liq. Cryst., 1983, Vol. 95, pp. 149–164
0026-8941/83/9502–0149/$18.50/0

Printed in the United States of America

Structure and Paramagnetism of Strong Charge-Transfer Complexes: 5.10-Dihydro-2.3.5.7.8.10-hexamethylphenazine-tetracyanoethylene (M_6P) (TCNE)

S. FLANDROIS,* K. LUDOLF,** H. J. KELLER,** D. NÖTHE,**
S. R. BONDESON,*** Z. G. SOOS,**** and D. WEHE**

**CNRS-CRPP, Domaine Universitaire, Talence, France*
***Anorganisch-Chemisches Institut der Universität Heidelberg, D-6900 Heidelberg 1, GFR*
****Department of Chemistry, University of Wisconsin, Stevens Point, WI 54481, USA*
*****Department of Chemistry, Princeton University, Princeton, N.J. 08544, USA*

(Received December 15, 1982)

The potent new donor 5.10-dihydro-2.3.5.7.8.10-hexamethylphenazine was synthesized and reacted with tetracyanoethylene to form a paramagnetic ionic charge transfer salt. The title compound ($C_{18}H_{22}N_2$) (C_6N_4), (M_6P) (TCNE), M_r = 394.51, crystallizes in the monoclinic space group $P2_1/n$ with a = 7.679(3) Å, b = 8.458(2) Å, c = 15.841(6) Å, β = 92.88(3)°, V = 1027.55 Å^3, d_c = 1.288 Mg · m^{-3}, and Z = 2. The planar M_6P^+ and $TCNE^-$ radical ions form mixed, regular stacks along b with a distance between M_6P^+ and $TCNE^-$ of 3.4(1) Å. Final refinement yielded R-indices of R = 0.092 and R_w = 0.058. Epr and static susceptibility data are interpreted in terms of novel disorder involving specific TCNE-allyl exchanges.

1. INTRODUCTION

The structural chemistry of charge-transfer (CT) complexes based on phenazine donors[1] provides new relations between the donor and acceptor properties of planar organic molecules and the resulting solid-state ionicity and physical properties. We have recently studied phenazine complexes of powerful π-acceptors like[2-4] TCNQ, [2.2′-(2.5-cyclohexadiene-

1.4-diylidene) bispropanedinitrile], and the even more powerful[5,6] $TCNQF_4$, [2,2′ (2.3.4.5-tetrafluoro-2.5-cyclohexadiene-1.4-diylidene) bispropanedinitrile]. Phenazine complexes of the smaller π-acceptor TCNE (tetracyanoethylene) have also been prepared.[7]

TCNE forms many CT complexes,[8-10] even with weak π-donors. Their structures typically show mixed...DADA... stacks.[10-13] Fully ionic alkali metal salts of TCNE are known.[14-16] Vapor deposition yields Na_nTCNE, with $n = 1, 2, 3$, and allows the Resonance Raman identification of $TCNE^-$, $TCNE^{2-}$, and $TCNE^{3-}$. CT complexes of TCNE with aromatic donors usually have largely neutral ground states. A rare ionic phenazine-TCNE complex is reported here.

Disubstituted phenazines are among the most powerful π-electron donors known.[5] The reaction between dimethylphenazine and TCNE yielded[7] three different solid products. The most stable one formed crystals for X-ray investigations and turned out[7] to be a condensation product rather than a CT complex. In order to obtain a pure CT salt of a 5.10-dihydro-5.10-dimethylphenazine derivative with TCNE, we subsequently synthesized[17] 5.10-dihydro-2.3.5.7.8.10-hexamethylphenazine (M_6P, 1).

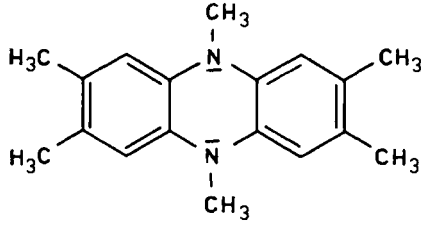

M_6P, 1

The 2, 3, 7 and 8 carbon positions in phenazine primarily attacked in the first step of the condensation reaction reported recently[7] are blocked by methyl groups in M_6P. Reaction with neutral TCNE yields a single product, a CT complex whose preparation, crystal structure, and paramagnetism is presented below. Quite aside from containing TCNE ion-radicals, the M_6P-TCNE paramagnetism has an unusual temperature dependence modeled in Section 3C.

2. CHEMICAL PREPARATIONS

A. 2.3.7.8.-Tetramethylphenazine[17]

The procedure for preparing this compound is analogous to the reported preparation of 2.3-dimethylphenazine.[18]

(i) 4.1 g red crystals (m.p. 103°C) of 4.5-dimethylbenzoquinone-1.2 were obtained by shaking a mixture of 5 g xylenol in 50 ml ether and a solution of 30 g potassium nitrosodisulfonate (Fremy's Salt) in 2500 ml of water with 200 ml of a 0.6 m aqueous KH_2PO_4 solution. After leaving the mixture standing for about 30 min at room temperature it was extracted with chloroform. The chloroform extract was dried with $CaCl_2$ and evaporated.

(ii) 6.8 g (0.05 mole) of the prepared 4.5-dimethylbenzoquinone-1.2 were further dissolved in about 500 ml toluene, combined with a solution of 6.8 g (0.05 mole) 4.5-dimethyl-1.2-diaminobenzene in 500 ml toluene and the resulting mixture was stirred for 12 h at room temperature. The reaction mixture was evaporated to about 500 ml and the brown powder which precipitates during evaporation was filtered off, washed with ether and recrystallized from ligroin, acetonitrile or toluene. 5 g yellow crystals of 2.3.7.8-tetramethylphenazine (m.p. 304°C) were obtained. Yield = 42%. The material was finally sublimed under vacuum at about 190°C.

Elemental analysis:	$C_{16}H_{16}N_2$	M_r: 236.22
Calc.: 81.32% C	6.82% H	11.85% N
Found: 81.29% C	7.32% H	11.83% N

B. 5.10-Dihydro-2.3.5.7.8.10-hexamethylphenazine

We follow a previous procedure[19] to reduce and directly to methylate phenazines:

To a suspension of 3.9 g (0.1 mole) potassium in about 500 ml ethane-1.2-dioledimethylether, which was dried over sodium hydride under a dry nitrogen atmosphere, 4.8 g (0.02 mole) of finely powdered 2.3.7.8-tetramethylphenazine were added and the mixture stirred for 48 h under a nitrogen atmosphere. (The suspension of the elemental potassium was obtained by using a *Herschberg* stirrer). 14.2 g (0.1 mole) CH_3I were dropped to the resulting red-violet solution. After the addition the excess elemental potassium was oxidized with ethanol and a saturated solution of NH_4Cl was added afterwards. The resulting emulsion was evaporated to dryness, suspended in 500 ml toluene and the residue filtered off. The obtained solution was concentrated by evaporation as far as possible. Using a 1:1 mixture of ether and toluene as eluent the product was chromatographed on a silica gel column. It is important for this last step (chromatography) to preheat the silica gel at 350°C in a high vacuum in order to remove all of the adsorbed oxygen. All solvents were saturated with nitrogen. Yield = 2 g (39%). The compound is obtained in yellow needles of m.p. 222°C.

Elemental analysis:	$C_{18}H_{22}N_2$	M_r: 266.38
Calc.: 81.16% C	8.32% H	10.52% N
Found: 81.38% C	8.60% H	10.78% N

C. M_6P-TCNE

266 mg (0.001 mole) of M_6P and 128 mg (0.001 mole) of TCNE were dissolved separately in 100 ml acetonitrile each and the solutions combined. Cooling to −20°C gives black needles of M_6P-TCNE. Yield: 110 mg (28%); m.p. above 300°C.

Elemental analysis:	$C_{24}H_{22}N_6$	M_r: 394.5
Calc.: 73.06% C	5.63% H	21.31% N
Found: 73.00% C	5.55% H	21.09% N

3. PHYSICAL MEASUREMENTS

A. X-ray investigation

Space group and unit cell dimensions were determined by rotation and Weissenberg photographs. Exact cell dimensions were obtained from an orientation matrix, derived from the setting angles of 19 independent reflections, centered on a Syntex-R3-diffractometer (Radiation MoK_α, Θ–2Θ scan, $2\Theta_{max} = 45°$, scan range 1.8°). Data collection was carried out on the diffractometer. An empirical absorption correction was applied to the data. The structure was solved by direct methods. The E-map showed 9 of the non-hydrogen atoms and a Fourier calculation with these atoms showed the remaining carbon and nitrogen atoms. A two-cycle refinement gave $R = 0.091$. The H-atoms were put in calculated positions and a 4-cycle refinement with weighted functions (weighting scheme: $W = 1/\sigma^2$ (F)) and anisotropic temperature factors for all non-hydrogen atoms yielded R-indices of $R = 0.092$ and $R_w = 0.058$. Reflections with $I < 0.5\sigma$ (I) were supressed. Final refinement gave $R = 0.100$ and $R_w = 0.058$.

B. Static susceptibility measurements

Static magnetic susceptibility investigations were carried out from 3 K to 300 K by the Faraday method in fields up 13.5 to kG. Measurements at several values of the magnetic field did not show any ferromagnetic contamination of the samples. The paramagnetism was obtained from the measured values in the usual way by substracting the core diamagnetism

measured on the separate constituents. The diamagnetic susceptibilities obtained for neutral M_6P and TCNE (-0.67 and -0.43×10^{-6} emu/g respectively) are in very good agreement with the values calculated from Pascal constants (-0.68 and -0.43).

C. EPR data

EPR spectra were taken at X- and Q-band on a Bruker B-ER 418 spectrometer equipped with an EIP 351.D microwave frequency counter and a Bruker NMR Gaussmeter for field calibration. Double integration of the EPR line for intensity determinations was performed on a Bruker ASPBCT-2000 computer by help of the standard EPRDTA program.

4. RESULTS

A. Crystal structure

Atomic coordinates and temperature factors are listed in Table I. Numbering scheme, bond distances and angles are shown in Figures 1 and 2. The M_6P^+ and the $TCNE^-$ ions are planar. They form mixed, regular stacks along b (Figure 3). The overlap of TCNE in (0, 0, 0) the M_6P in (0, ½, 0) and TCNE in (0, 1, 0) is shown in Figure 4. The interplanar distance is 3.4(1) Å. The TCNE in Figure 4 overlaps an allyl fragment, with a noticeable enlarged thermal ellipsoid for the central carbon [C(5) and C′(5)]. The stacking type resembles those of the TCNE molecular complexes with the donors naphthalene[11] and perylene,[12] but the overlap patterns between the donors and TCNE are quite different. The central C—C distance in the TCNE moiety (1.370(11) Å) is the longest observed so far in TCNE charge transfer complexes (Table II). Since all the solids mentioned in Table II are diamagnetic (no detectable EPR signals) the comparatively long central C—C distance in TCNE of M_6P-TCNE suggests an *ionic* ground state. The interplanar distances along the mixed stacks are comparatively large (3.4 Å). As also noted in perylenium salts[20] the higher ionicity of M_6P-TCNE does not lead to closer interplanar contacts. The higher ionicity and TCNE-allyl contacts are new structural features in M_6P-TCNE.

B. Paramagnetic susceptibility and EPR

The paramagnetic part of the M_6P-TCNE susceptibility is shown in Figure 5 as $\log \chi(T)/\chi_c$ vs $\log T$. Here χ_c is the Curie contribution for two moles of $s = ½$ spins,

TABLE I

Atomic coordinates and temperature factors of M_6P-TCNE

Atom	X/A	Y/B	Z/C	K	U11	U22	U33	U23	U13	U12	U(Equiv)
C4	.29071	.76965	.13141	1.0000	.0520	.0422	.0331	−.0141	.0027	.0074	.0424
	.00077	.00067	.00036	.0000	.0048	.0046	.0040	.0036	.0037	.0039	.0026
C9	.44695	.86522	.15624	1.0000	.0458	.0572	.0630	−.0220	−.0070	−.0076	.0557
	.00079	.00082	.00039	.0000	.0048	.0050	.0050	.0044	.0037	.0042	.0029
H9A	.52247	.81438	.20539	1.0000	.0500						
	.00584	.00560	.00257	.0000	.0000						
H9B	.42553	.98076	.17168	1.0000	.0500						
	.00600	.00517	.00276	.0000	.0000						
H9C	.55050	.85758	.12209	1.0000	.0500						
	.00589	.00611	.00270	.0000	.0000						
C10	.14452	.83069	.26581	1.0000	.0814	.0699	.0450	−.0158	.0040	−.0124	.0654
	.00095	.00092	.00040	.0000	.0069	.0060	.0054	.0046	.0045	.0052	.0036
H10A	.25044	.80785	.29583	1.0000	.0500						
	.00632	.00625	.00313	.0000	.0000						
H10B	.06319	.78817	.30665	1.0000	.0500						
	.00624	.00576	.00288	.0000	.0000						
H10C	.15015	.94051	.25977	1.0000	.0500						
	.00468	.00480	.00229	.0000	.0000						
C5	.28673	.69052	.05244	1.0000	.0707	.0716	.0843	.0144	.0065	.0096	.0754
	.00076	.00063	.00033	.0000	.0048	.0046	.0048	.0039	.0040	.0040	.0027
H5	.41309	.72059	−.00093	1.0000	.0500						
	.00553	.00501	.00271	.0000	.0000						
C6	.14101	.59196	.02380	1.0000	.0253	.0375	.0474	.0098	−.0037	.0015	.0369
	.00071	.00065	.00034	.0000	.0037	.0044	.0040	.0035	.0034	.0032	.0024
C1	.00078	.57746	.07780	1.0000	.0297	.0427	.0378	.0042	.0002	.0006	.0368
	.00067	.00062	.00030	.0000	.0037	.0042	.0036	.0034	.0032	.0034	.0022
C2	.00720	.65869	.15561	1.0000	.0342	.0435	.0372	−.0055	.0023	−.0001	.0383
	.00071	.00067	.00035	.0000	.0041	.0043	.0039	.0036	.0033	.0035	.0024

N7	.13923	.51390	−.05298	1.0000	.0319	.0393	.0337	−.0090	.0088	−.0008	.0347
	.00057	.00052	.00024	.0000	.0030	.0034	.0031	.0027	.0026	.0028	.0018
C8	.28811	.52761	−.10573	1.0000	.0494	.0650	.0506	−.0199	.0245	−.0189	.0542
	.00082	.00080	.00042	.0000	.0049	.0059	.0042	.0045	.0040	.0039	.0029
H8A	.24562	.56152	−.16819	1.0000	.0500						
	.00578	.00552	.00256	.0000	.0000						
H8B	.33834	.43431	−.11732	1.0000	.0500						
	.00680	.00553	.00315	.0000	.0000						
H8C	.35861	.60409	−.09696	1.0000	.0500						
	.00639	.00577	.00322	.0000	.0000						
C3	.14806	.75062	.18159	1.0000	.0570	.0254	.0291	−.0072	.0009	.0152	.0372
	.00074	.00062	.00033	.0000	.0049	.0041	.0036	.0033	.0034	.0036	.0025
C11	.02471	.04929	.03278	1.0000	.0600	.0457	.0510	−.0053	−.0088	.0194	.0526
	.00080	.00068	.00032	.0000	.0047	.0052	.0050	.0034	.0037	.0041	.0029
C12	.18672	.13773	.02764	1.0000	.0564	.0506	.0477	−.0030	−.0016	.0039	.0517
	.00086	.00079	.00037	.0000	.0049	.0049	.0045	.0039	.0040	.0043	.0028
N13	.31432	.20826	.02861	1.0000	.0669	.0640	.0563	.0006	−.0025	−.0223	.0626
	.00071	.00062	.00033	.0000	.0045	.0045	.0039	.0032	.0035	.0036	.0025
C14	−.07710	.07690	.10461	1.0000	.0603	.0454	.0559	−.0020	−.0016	.0065	.0540
	.00084	.00078	.00037	.0000	.0049	.0046	.0046	.0041	.0040	.0040	.0027
N15	−.15253	.09954	.16278	1.0000	.0918	.0736	.0628	.0000	.0141	.0123	.0757
	.00076	.00068	.00031	.0000	.0052	.0045	.0042	.0040	.0037	.0040	.0027
H2	−.10122	.65715	.18935	1.0000	.0500						
	.00534	.00463	.00235	.0000	.0000						

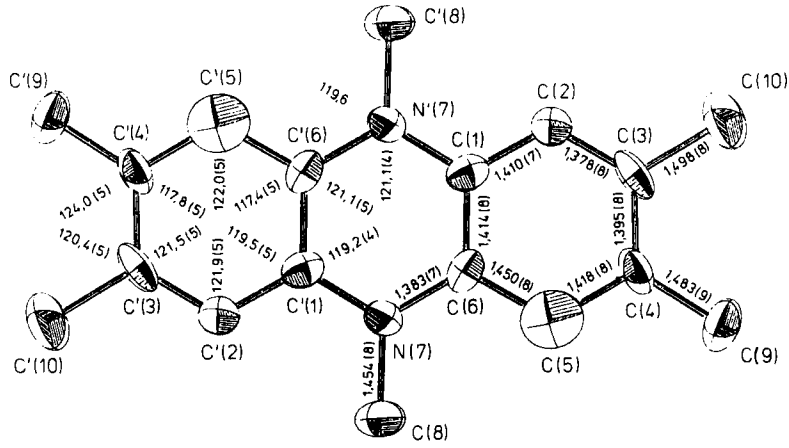

FIGURE 1 Numbering scheme, bond distances and bond angles in the M_6P^+-radical cation.

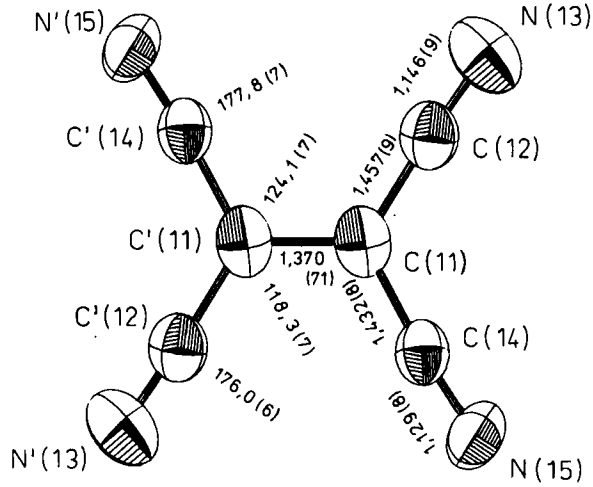

FIGURE 2 Numbering scheme, bond distances and bond angles of the $TCNE^-$ radical anion.

$$\chi_c = 2N_A\left(\frac{g^2\mu_B^2}{4kT}\right) \tag{1}$$

where N_A is Avogadro's number, $g \sim 2.0030$ is close to the free-electron g-factor, μ_B is the Bohr magneton, k is Boltzmann's constant, and T is the absolute temperature. According to the fluctuation-dissipation theorem, the effective concentration of free spins, $\chi(T)/\chi_c$, in Figure 5, gives the sum

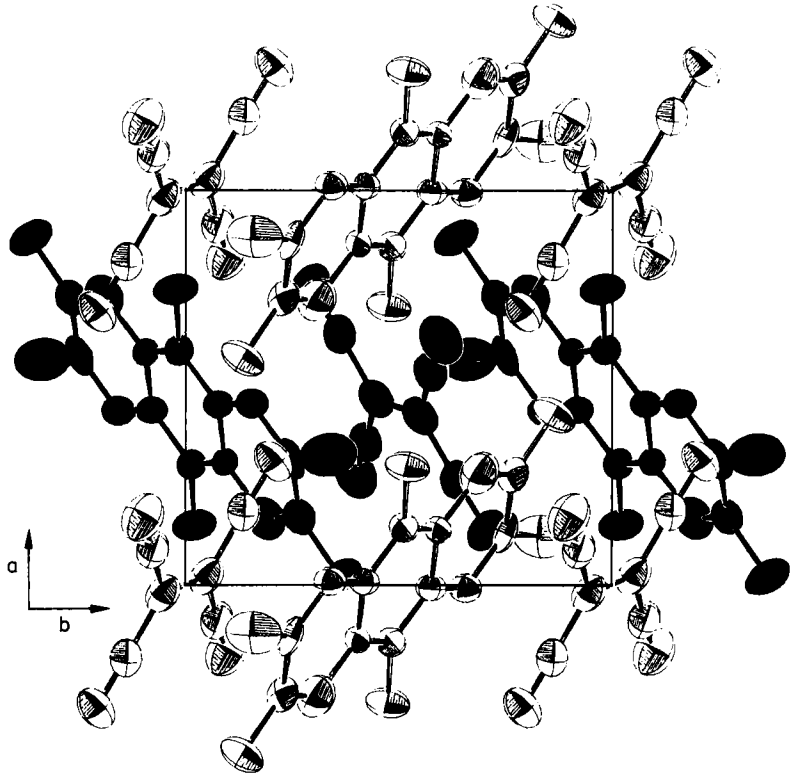

FIGURE 3 Projection of three chain segments of the mixed stacks in M_6P-TCNE onto the *ab* plane.

of all static spin correlations.[2] We immediately infer either antiferromagnetic interactions among M_6P^+ and $TCNE^-$ ion radicals or possibly a partly-ionic ground state. The rapid increase of $\chi(T)/\chi_c$ around 300 K is more indicative of antiferromagnetic exchanges $J/k < 300$ K, however, and such a model is pursued below.

The EPR spectrum of polycrystalline M_6P-TCNE consists of a single, asymmetric line at $g = 2.0030$. The peak-to-peak width of the derivative line is 1.2 G, which is again indicative of substantial exchange narrowing. The temperature dependence of the EPR intensity between 113 and 294 K is shown in Figure 6. The temperature dependence of $I(T)$ parallels the static data in Figures 5 to 230 K and confirms the plateau region below 140 K. Above 220 K the EPR intensity increases slightly more rapidly than the static susceptibility, presumably due to inaccuracies in doubly integrating the EPR spectrum.

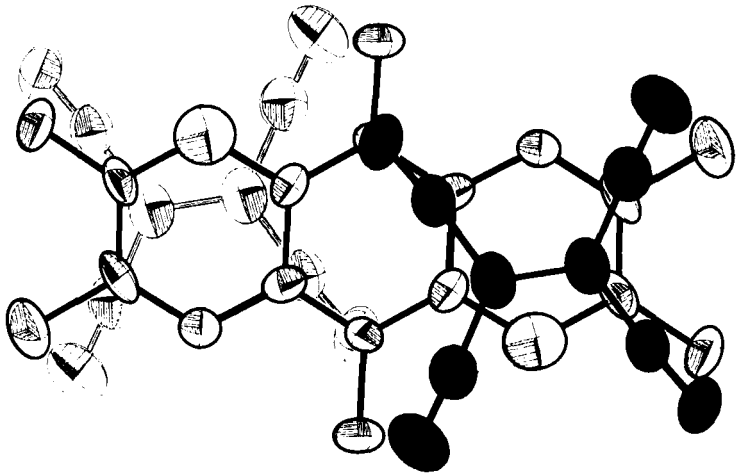

FIGURE 4 *Overlap pattern between a "sandwiched" M_6P ion and its direct TCNE neighbors at (0, 0, 0) and (0, 1, 0). (Black ellipsoids are drawn for atoms above, shaded ellipsoids for the atoms below the M_6P^+ plane).*

The line asymmetry of powder samples becomes more pronounced at lower temperature, though the width is almost constant. We associate this with g-tensor anisotropy. This was verified through the linear frequency dependence of the width at Q band. Single-crystal X-band spectra at room

TABLE II

Characteristic distances in TCNE charge transfer complexes

	a(Å)	b(Å)	c(Å)	Ref.
Neutral TCNE	1.339(8)	1.441(5)	1.134(5)	26
Skatole-TCNE	1.290(7)	1.446(7)	1.131(7)	13
		1.450(7)	1.125(6)	
Pyrene-TCNE	1.309(12)	1.468(13)	1.118(12)	27
[3.3]-Paracyclophane-TCNE	1.348(7)	1.469(5)	1.141(10)	28
Naphthalene-TCNE	1.351(14)	1.426(7)	1.131(8)	11a
Perylene-TCNE	1.359(10)	1.456(11)	1.135(12)	12
		1.438(8)	1.105(11)	
M_6P-TCNE	1.370(11)	1.457(9)	1.146(9)	this
		1.432(8)	1.129(8)	work

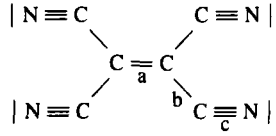

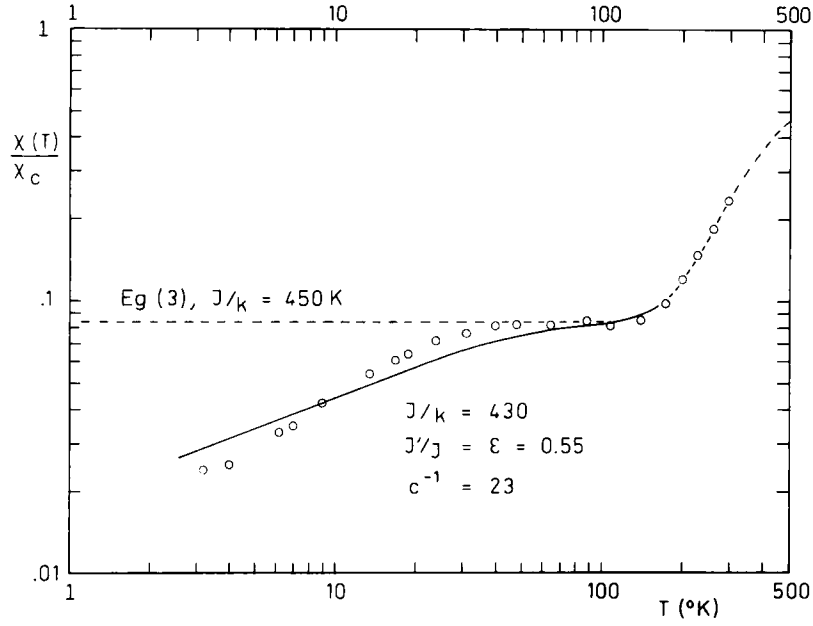

FIGURE 5 Temperature dependence of the static susceptibility χ. The plot shows log $\chi(T)/\chi_c$ vs log T.

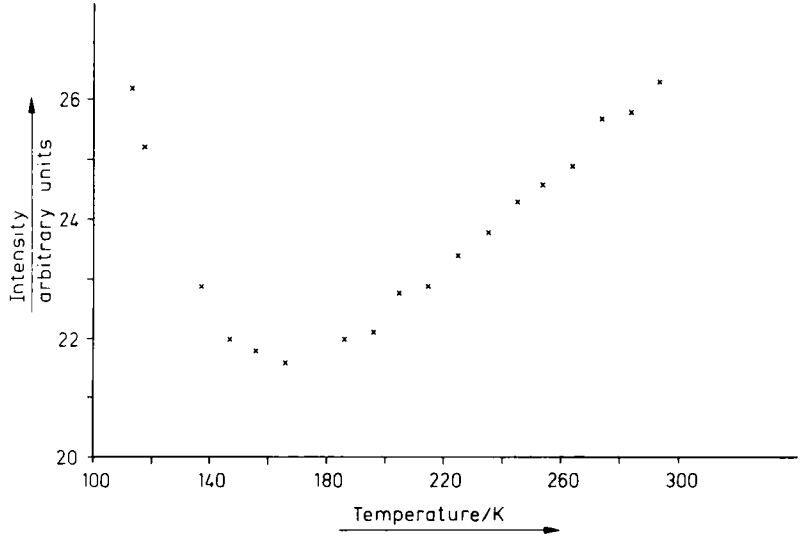

FIGURE 6 Temperature dependence of the BPR intensity of M_6P-TCNE.

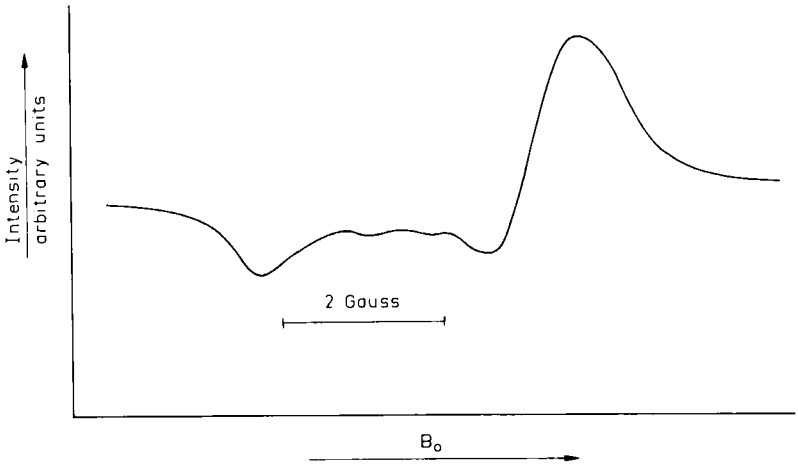

FIGURE 7 Q-band EPR spectrum of polycrystalline M_6P-TCNE.

temperature yield the principal values of $g_\perp = 2.0027$, $g_\parallel = 2.0034$. While the absolute numbers are typical of ion-radical organic solids,[1,22] this is not the case for the sequence of $g_\perp$ and $g_\parallel$ as shown by the Q-band powder spectrum in Figure 7. Normally one finds $g_\parallel \sim 2.0023 < g_\perp$. This means that we do not observe the "molecular" g-values of the individual $TCNE^-$ or M_6P^+ moieties, but "crystal" g-values, which are determined by the lattice arrangement and exchanges. So we conclude that a rapid exchange of unpaired electrons between the two different stacks leads to an averaging of their g-values. As a lower limit for the exchange frequency one calculates a value of about 10 MHz.

No fine structure splittings were found between 130 and 350 K, in contrast with one of the M_6P-TCNE products.[7] Any triplet spin excitons are consequently in the high-temperature region of collapsed fine-structure splittings.

C. Disorder model for the susceptibility

The novel paramagnetism of the ion-radical solid M_6P-TCNE is shown in Figure 5. The power-law behavior below 40 K indicates disordered exchanges[21] for about 8% of the M_6P and TCNE spins and thermal decoupling in the plateau region between 40 and 140 K. The rapid increase above 140 K suggests stronger antiferromagnetic exchanges for the remaining spins. We introduce the exchange Hamiltonian

$$H = \sum_n 2J_n\,(\mathbf{S}_n \cdot \mathbf{S}_{n+1} - 1/4) \tag{2}$$

for modeling $\chi(T)$. Here $J_n > 0$ describes antiferromagnetic coupling between successive $s = 1/2$ sites associated with $TCNE^-$ at even n and M_6P^+ at odd n. The mixed regular stack in Figure 3 suggests $J_n = J$ in Eq. (2). That choice is inconsistent, however, with the data in Figure 5, which does not follow the Bonner-Fisher[23] solution of Eq. (2) for $J_n = J$.

As already mentioned, the TCNE-M_6P overlap suggests specific TCNE-allyl interactions, which may be induced by defects on adjacent stacks. For our purposes, specific interactions translate into large J, as shown schematically in Figure 8 by dashed lines. Each TCNE has one J and a weaker exchange $J' < J$. Perfect alternation of J and J' along the stack is again inconsistent with the $\chi(T)$ data. We postulate instead some M_6P with two strong exchanges, the trimers in Figure 8, and others with two J', the monomers. Now J and J' are equally probable along the stack, but no more than two consecutive like exchanges can occur. It also follows that monomers and trimers alternate along the stack, separated by an arbitrary number of dimers with one J and one J' in Figure 8.

We define c to be the concentration of either monomers or trimers. The remaining $(1 - 4c)N$ spins yield a dimer density of $(1 - 4c)/2$. The simple $J' \to 0$ limit yields a singlet-triplet splitting of $2J$ for dimers, and a doublet for monomers and trimers, which also have an excited doublet at $2J$ and a quartet at $3J$. The $J' = 0$ density of free spins is

$$\frac{\chi^{(0)}(T)}{\chi} = 2c + \frac{8c}{2 + z + z^3} + \frac{4(1 - 4c)}{z + z^2} \tag{3}$$

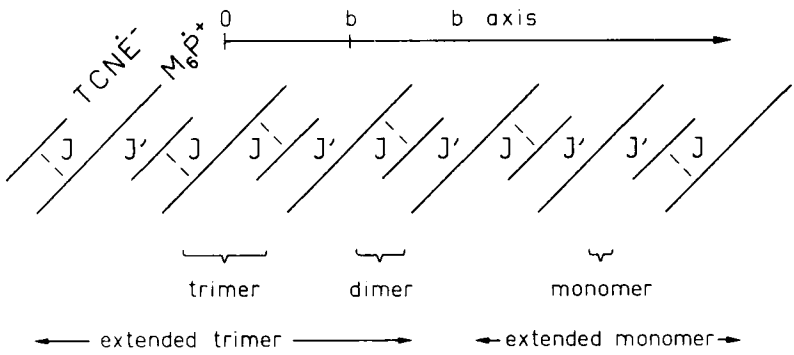

FIGURE 8 Schematic drawing of the exchanges J and J' along a M_6P-TCNE chain.

with $z = \exp(J/kT)$. The dashed line in Figure 5 is based on Eq. (3) with $c^{-1} = 24$ from the plateau and $J/k = 450$ K for the upturn above 150 K. The thermally decoupled spins are associated with some 4% monomers and 4% trimers produced by an unspecified defect mechanism.

Turning on $J' > 0$ couples trimer and monomer spins and ultimately reduces $\chi(T)/\chi_c$. The general procedure has been discussed[21,24] in connection with $Q(TCNQ)_2$. In effect, we renormalize at low T to regain Eq. (2) for $s = \frac{1}{2}$ sites associated with monomers and trimer ground states, while the effective exchanges J_n now describe the attenuation of intervening dimers frozen into their singlet ground state.

Shifting a single TCNE in Figure 8 converts a monomer-trimer pair into a stabler pair of dimers. In general $p + 1$ intervening TCNE must shift in concert to form $p + 2$ dimers, as seen in Figure 8 for $p = 2$. The energy gain is small, concerted motion becomes improbable, and crystal defects may also help to freeze in the disorder. We assume for modeling purposes a dimer on either side of the monomer and trimer, as indicated by the extended paramagnetic centers in Figure 8. The remaining $(1 - 12c)/2$ dimer density is distributed randomly, according to the normalized probability

$$f(p) = a(1 - a)^p \tag{4}$$

for $p = 0, 1, 2, \ldots$ dimers between extended paramagnetic centers. It follows that a in Eq. (4) is the fraction of extended paramagnetic centers along the chain,

$$a = 2c[2c + (1 - 12c)/2]^{-1} \tag{5}$$

The strongest coupling involves adjacent paramagnetic centers, or $p = 0$. Each additional intervening dimer attenuates the exchange. Thus Eq. (4) leads to a wide distribution of small effective exchanges.

Finite segments of Eq. (2) are readily solved[21] for arbitrary J_n. The ground state spin densities of extended monomers and trimers were found for various $\varepsilon = J'/J$. The $p(m)p(t)$ entry in Table III gives the exchange,

Table III

Effective exchanges $\varepsilon J p(m)p(t)$ for adjacent extended monomers and dimers and reduction factors $g_p(\varepsilon)$ for $p = 1,2,3$, intervening dimers.

	$\varepsilon = 0.01$	0.25	0.55
$p(m)p(t)$	1.69×10^{-5}	0.0139	0.0779
g_1	0.2522	0.3098	0.3770
g_2	0.0636	0.0960	0.1421
g_3	0.0160	0.0297	0.0536

$J'p(m)p(t)$, for adjacent paramagnetic centers. The effective exchanges for $p = 0, 1, 2$, and 3 were found as before[21] from the exact singlet-triplet splittings. As shown in Table III, each dimer reduces the splitting by a factor $g(\varepsilon)$, that reduces for $\varepsilon \to 0$ to 4^{-1}. The effect of longer dimer sequences is then readily estimated as $[g(\varepsilon)]^p$. The probabilities in Eq. (4) are exact while the perturbation procedure for effective exchanges holds for small $\varepsilon = J'/J$. Its accuracy for $\varepsilon \sim 0.5$, as needed below, has not been demonstrated.

We obtained $\chi(T)/\chi_c$ below 100 K by generating replicas[21] with eight extended paramagnetic centers according to Table II and Eq. (4). All $p > 7$ exchanges were omitted as separating replicas. Averaging over $R = 100$ replicas converges satisfactorily down to $T \sim 1$–2 K. The solid curve in Figure 5 has $c^{-1} = 23$, $\varepsilon = 0.55$, and $J/k = 430$ K. It is indistinguishable above 150 K from the simpler curve based on Eq. (3) and a slightly higher J.

The fit below 100 K is not quantitative, although the expected power law for disordered exchanges is clearly seen. The large value of ε, the rather arbitrary definition of extended paramagnetic centers, and the preliminary nature of the present model do not warrant additional parametrization. A better plateau could be produced by assuming at least three, instead of two, dimers between the actual trimers and monomers. Longer segments are needed to minimize the effects of large ε by including more J' contributions directly. Such computations will be needed if the M_6P-TCNE data is extended below 1 K to the mK regime already studied[21,25] in $Q(TCNQ)_2$.

5. SUMMARY

The newly-prepared, powerful π-donor M_6P forms a rare ionic charge-transfer complex with the π-acceptor TCNE. The reported M_6P-TCNE structure consists of mixed regular stacks along the b axis, with a TCNE overlap of an allyl fragment rather than a phenyl ring. The novel paramagnetism of M_6P-TCNE in Figure 5 has been modeled by disordered exchanges based on strong TCNE-allyl contacts. Additional structural evidence, as well as other examples, are needed to confirm such a disordered-exchange model.

Acknowledgment

Z. G. Soos thanks the Guggenheim Foundation for a fellowship and the Department of Physics, University of California, Los Angeles for its warm hospitality in 1981–82; the support of NSF-DMR-8105010 is gratefully acknowledged.

The work in Heidelberg was supported by DFG (Ke 135/18 and Ke 135/25), Fonds der Chemischen Industrie and Stiftung Volkswagenwerk (Az.: I/37244). The necessary personal contacts between the groups were made possible by a NATO Research Grant (No. 137.81).

References

1. H. J. Keller and Z. G. Soos in "Extended Linear Chain Compounds," ed. J. S. Miller, Vol. 4, Plenum Press, New York, in print.
2. H. Endres, H. J. Keller, W. Moroni, and D. Nöthe, *Acta Cryst.*, **B36**, 1435 (1980).
3. R. H. Harms, H. J. Keller, D. Nöthe, M. Werner, D. Gundel, H. Sixl, and R. M. Metzger, *Mol. Cryst. Liq. Cryst.*, **65**, 179 (1981).
4. K. Dietz, H. Endres, H. J. Keller, W. Moroni, and D. Wehe, *Z. Naturforsch.*, **37b**, 437 (1982).
5. Z. G. Soos, H. J. Keller, K. Ludolf, J. Queckbörner, D. Wehe, and S Flandrois, *J. Chem. Phys.*, **74**, 5287 (1981).
6. R. M. Metzger, N. E. Heimer, D. Gundel, H. Sixl, R. H. Harms, H. J. Keller, D. Nöthe, and D. Wehe, *J. Chem. Phys.*, in print.
7. K. Dietz, H. J. Keller, D. Nöthe, and D. Wehe, *J. Amer. Chem. Soc.*, in print.
8. R. E. Merrifield and W. D. Phillips, *J. Amer. Chem. Soc.*, **80**, 2778 (1958).
9. D. J. Cram and R. H. Bauer, *J. Amer. Chem. Soc.*, **81**, 5971 (1959).
10. E. Adam, M. Rosenblum, S. Sullivan, and T. N. Margulis, *J. Amer. Chem. Soc.*, **89**, 4541 (1967).
11. a) R. M. Williams and S. C. Wallwork, *Acta Cryst.*, **22**, 899 (1967); b) D. Lee and S. C. Wallwork, *Acta Cryst.*, **B34**, 3604 (1978).
12. I. Ikemoto, K. Yakushi, and H. Kuroda, *Acta Cryst.*, **26B**, 800 (1970).
13. E. E. Castellano, B. E. Rivero, A. D. Podjarny, and M. E. Roselli, *Acta Cryst.*, **B36**, 1726 (1980).
14. O. W. Webster, W. Mahler, and R. E. Benson, *J. Org. Chem.*, **25**, 1470 (1960).
15. M. S. Khatkale and J. P. Devlin, *J. Phys. Chem.*, **83**, 1636 (1979).
16. J. J. Hinkel and J. P. Devlin, *J. Chem. Phys.*, **58**, 4750 (1973).
17. K. Ludolf, Dissertation, University of Heidelberg, 1980.
18. H. J. Teuber and G. Staiger, *Chem. Ber.*, **88**, 802 (1955).
19. H. Gilman and J. Dietrich, *J. Amer. Chem. Soc.*, **79**, 6178 (1957).
20. D. Wehe, Dissertation, University of Heidelberg, 1981.
21. S. R. Bondeson and Z. G. Soos, *Phys. Rev.*, **B22**, 1793 (1980); *Solid State Commun.*, **35**, 11 (1980).
22. P. L. Nordio, Z. G. Soos, and H. M. McConnell, *Ann. Rev. Phys. Chem.*, **17**, 237 (1966).
23. J. C. Bonner and M. E. Fisher, *Phys. Rev.*, **135**, 640 (1964); a useful power-series fit for $\chi(T)$ is given by J. B. Torrance, Y. Tomkiewicz, and D. B. Silverman, *Phys. Rev.*, **B15**, 4738 (1977).
24. Z. G. Soos and S. R. Bondeson, *Solid State Commun.*, **39**, 289 (1981).
25. W. G. Clark in "Physics in One Dimension," (Springer Series in Solid State Sciences, Vol. 23, 1981, eds. J. Bernasconi and T. Schneider, Springer, Berlin), pp. 289–301.
26. D. A. Bekoe and K. N. Trueblood, *Z. Kristallogr.* **113**, 1 (1960).
27. I. Ikemoto and H. Kuroda, *Acta Cryst.*, **24B**, 383 (1968).
28. J. Bernstein and K. N. Trueblood, *Acta Cryst.*, **B27**, 2078 (1971).